



Recombinant sclerostin inhibits bone formation *in vitro* and in a mouse model of sclerosteosis



Timothy Dreyer^{a,b,*}, Mittal Shah^b, Carl Doyle^b, Kevin Greenslade^b, Mark Penney^b, Paul Creeke^b, Apoorva Kotian^b, Hua Zhu Ke^{b,1}, Vinny Naidoo^a, Gill Holdsworth^b

^a University of Pretoria, Pretoria, South Africa

^b UCB Pharma, Slough, UK

ARTICLE INFO

Keywords:

Bone formation
Sclerosteosis
Sclerostin
SOST
Therapy

Background: Sclerosteosis, a severe autosomal recessive sclerosing skeletal dysplasia characterised by excessive bone formation, is caused by absence of sclerostin, a negative regulator of bone formation that binds LRP5/6 Wnt co-receptors. Current treatment is limited to surgical management of symptoms arising from bone overgrowth. This study investigated the effectiveness of sclerostin replacement therapy in a mouse model of sclerosteosis.

Methods: Recombinant wild type mouse sclerostin (mScl) and novel mScl fusion proteins containing a C-terminal human Fc (mScl hFc), or C-terminal human Fc with a poly-aspartate motif (mScl hFc PD), were produced and purified using mammalian expression and standard chromatography methods. *In vitro* functionality and efficacy of the recombinant proteins were evaluated using three independent biophysical techniques and an *in vitro* bone nodule formation assay. Pharmacokinetic properties of the proteins were investigated *in vivo* following a single administration to young female wild type (WT) or SOST knock out (SOST^{-/-}) mice. In a six week proof-of-concept *in vivo* study, young female WT or SOST^{-/-} mice were treated with 10 mg/kg mScl hFc or mScl hFc PD (weekly), or 4.4 mg/kg mScl (daily). The effect of recombinant sclerostin on femoral cortical and trabecular bone parameters were assessed by micro computed tomography (μ CT).

Results: Recombinant mScl proteins bound to the extracellular domain of the Wnt co-receptor LRP6 with high affinity (nM range) and completely inhibited matrix mineralisation *in vitro*. Pharmacokinetic assessment following a single dose administered to WT or SOST^{-/-} mice indicated the presence of hFc increased protein half-life from less than 5 min to at least 1.5 days. Treatment with mScl hFc PD over a six week period resulted in modest but significant reductions in trabecular volumetric bone mineral density (vBMD) and bone volume fraction (BV/TV), of 20% and 15%, respectively.

Conclusion: Administration of recombinant mScl hFc PD partially corrected the high bone mass phenotype in SOST^{-/-} mice, suggesting that bone-targeting of sclerostin engineered to improve half-life was able to negatively regulate bone formation in the SOST^{-/-} mouse model of sclerosteosis.

The translational potential of this article: These findings support the concept that exogenous sclerostin can reduce bone mass, however the modest efficacy suggests that sclerostin replacement may not be an optimal strategy to mitigate excessive bone formation in sclerosteosis, hence alternative approaches should be explored.

1. Introduction

Sclerosteosis (OMIM accession number 269500) is a rare, autosomal recessive, high bone mass condition with approximately 100 cases reported worldwide, of which two thirds are of Afrikaner descent from South Africa [1,2]. In contrast to many osteopetrotic high bone mass conditions, sclerosteosis is associated with increased bone formation (hyperostosis), rather than defects in bone resorption. Cutaneous or bony

syndactyly and dysplastic or absent nails are the earliest post-natal indicators of the condition. Further clinical features include skeleton-wide increased bone mineral density (BMD), thicker than normal trabeculae and cortices, and generalised skeletal overgrowth that results in a tall stature, recurrent facial palsy, hearing loss and potentially lethal elevated intracranial pressure [3–8]. The condition currently has no available treatment and disease management is limited to difficult and protracted surgical decompression of entrapped cranial nerves and elevated

* Corresponding author. 72 Jan K Marais Avenue Malanshof Randburg, 2194, South Africa.

E-mail address: u15413706@tuks.co.za (T. Dreyer).

¹ Current address: Angitia Biopharmaceuticals, Guangzhou, China

<https://doi.org/10.1016/j.jot.2021.05.005>

Received 8 March 2021; Received in revised form 17 May 2021; Accepted 20 May 2021

intracranial pressure [4,7]. Furthermore, bone regrowth often occurs post-surgery and may cause recurrence of symptoms, necessitating repeat surgeries. Reducing bone formation in sclerosteosis through pharmacological strategies could reduce the incidence of elevated intracranial pressure and cranial nerve entrapment and hence would be highly beneficial to patients.

Sclerosteosis is caused by the absence of sclerostin expression, and independent groups have reported various loss of function mutations in the *SOST* gene in chromosome location 17q12-q21. These nonsense, missense or frameshift mutations alter the expression and processing of the *SOST* transcript, resulting in loss of functional sclerostin [2,9–12]. The canonical Wnt/ β -catenin signalling pathway plays an essential role in developmental regulation and adult bone homeostasis, and is activated upon binding of Wnt to the low-density lipoprotein receptor-related proteins 5 and 6 (LRP5/6) Wnt co-receptors [13,14]. Sclerostin, primarily expressed by osteocytes, regulates the canonical Wnt/ β -catenin pathway by antagonising Wnt signalling in bone through high-affinity binding to the extracellular domains of LRP4/5/6 [13]. Loss of sclerostin thus leads to enhanced canonical Wnt signalling in the skeleton, resulting in the excessive bone formation characteristic of sclerosteosis [15].

Replacing absent sclerostin in sclerosteosis patients with exogenous protein could potentially inhibit Wnt/ β -catenin signalling in the skeleton, thereby safely reducing the excessive bone formation. Protein replacement therapies have previously been used to treat anaemia and haemophilia A or B by administering recombinant erythropoietin and factors VIII or IX, respectively [16–18] providing confidence that such an approach could be effective for sclerosteosis. Preclinical proof of concept experiments that explore the feasibility of protein replacement strategies are greatly aided by good translational animal models. Sclerostin-deficient *SOST* knockout (*SOST*^{-/-}) mice exhibit increased bone mass throughout the skeleton in early life, which is sustained as mice age [15,19], making *SOST*^{-/-} mice an appropriate model in which to test the concept of sclerostin replacement as a strategy to mitigate the excessive bone formation of sclerosteosis.

This study therefore investigated the hypothesis that administration of recombinant sclerostin protein may reduce the excessive bone phenotype in a *SOST*^{-/-} mouse model of sclerosteosis.

2. Materials and methods

2.1. Plasmid cloning

All recombinant mouse sclerostin constructs (mScl, mScl hFc and mScl hFc PD) were cloned via restriction enzyme digest into a proprietary pMH expression vector containing a modified human cytomegalovirus (CMV) promoter and enhancer for transient expression of inserted gene sequences and a kanamycin resistance gene for antibiotic selection (UCB Celltech). For the fusion proteins, IgG1 hFc (DNA2.0) was fused in-frame downstream of the final codon of mScl and an octa-aspartate motif (poly-aspartate, PD) was added at the hFc C-terminus for the mScl hFc PD construct. DNA fragments (mScl, hFc and hFc PD) were obtained from DNA2.0.

2.2. Protein expression and purification

Recombinant mScl proteins were transiently expressed in an Expi293 Expression system (Thermo Fisher Scientific). HEK293 (5 L) cultures were centrifuged (1.5 h at 4 °C and 13000×g) and vacuum filtered supernatant was loaded onto chromatography columns on an ÄKTA Pure chromatography system (GE Healthcare Life Sciences). Native mScl was purified on a RESOURCE S cation exchange chromatography (CEC) column (GE Healthcare Life Sciences), equilibrated with 50 mM MES, 100 mM NaCl, pH 6, and eluted by linear gradient with 50 mM MES, 500 mM NaCl, pH 6. Eluates were subsequently purified by gel filtration on a HiLoad 26/600 Superdex 75 pg column (GE Healthcare Life Sciences) in

10 mM phosphate buffered saline (PBS). The mScl hFc and mScl hFc PD constructs were purified by affinity chromatography using a HiTrap Protein A HP (5 mL) column (GE Healthcare Life Sciences) and eluted by linearly increasing pH with 0.1 M citric acid pH 2. Eluate pH was adjusted to 7 with 1 M Tris-HCl pH 8.5 and were further purified by gel filtration on a HiLoad 26/600 Superdex 200 pg column (GE Healthcare Life Sciences) in 10 mM PBS, followed by CEC on a RESOURCE S column. Glycerol (10%) was added to purified protein and an Endosafe-PTS system (Charles River) used to measure sample endotoxin levels. To visualise protein bands, gels were stained with InstantBlue Protein Stain (Expedeon) and imaged with an ImageQuant LAS 4000 camera system (GE Healthcare Life Sciences).

Protein structure was analysed by N-terminal sequencing. Denatured proteins were transferred from SDS PAGE gels to a polyvinylidene fluoride membrane and stained with Ponceau S solution (Merck). Bands of interest were excised and individually applied to reaction cartridges on a Precise Protein Sequencing System (Life Technologies), followed by subjection to 13 cycles of Edman Chemistry including 2x blanks and 1x PTH-amino acid standard. Data was analysed using SequencePro Data Analysis Application (Applied Biosystems).

2.3. Isothermal titration calorimetry

Recombinant protein samples were desalted using 7K molecular weight cut-off Zeba Spin Desalting Columns (Thermo Fischer Scientific) and diluted to 20 μ M in Dulbecco's phosphate-buffered saline (DPBS). Isothermal titration calorimetry (ITC) data was measured at 25 °C using a MicroCal PEAQ-ITC instrument (Malvern Instruments Ltd). A 20 μ M solution of recombinant mScl was added to the sample cell and titration was performed with ten 4 μ L injections (0.4 μ L first injection) of 111 μ M LRP6-E1E2 [20] (UCB). Each binding test was performed in triplicate and data were fitted to a single site binding model and analysed using MicroCal PEAQ-ITC Analysis Software (Malvern Instruments Ltd). Further information on two orthogonal techniques (surface plasmon resonance competition assay and microscale thermophoresis) is provided in the supplemental data.

2.4. In vitro bone nodule formation assay

MC3T3-E1 Subclone 14 mouse pre-osteoblasts (ATCC CRL-2594) in complete (CT) growth medium (Minimum Essential Medium Alpha (Thermo Fischer Scientific) containing 2 mM L-Glutamine, Ribonucleosides, Deoxyribonucleosides, and 10% foetal bovine serum) were plated at 6020 cells/cm² in 24 well culture plates and maintained at 37 °C and 5% CO₂. After 48 h, media was replaced with osteogenic (OM) media (complete growth medium supplemented with 50 μ g/mL ascorbate-2-phosphate and 10 mM β -glycerophosphate) and cells were treated with 50 nM recombinant mScl. Vehicle controls were treated with PBS, whilst antibody (Ab) controls were co-treated with 50 nM recombinant mScl and 230 nM sclerostin neutralising (Anti-Scl Ab [21]) (UCB) or irrelevant isotype control Abs (Control Ab) (UCB). Cells were maintained at 37 °C and 5% CO₂ and treatments were repeated with new media every 48 h. Upon mineralisation, cells were fixed with formalin and stained with 40 mM Alizarin Red S pH 4 (Sigma Aldrich) to detect mineralisation. For quantitation, stained mineral was destained with 10% (w/v) cetylpyridinium chloride (CPC) and absorbance was measured at 570 nm using a Synergy 2 Multi-Mode Microplate Reader (BioTek).

2.5. In vivo study design

Female *SOST*^{-/-} mice and wild type C57/BL6 littermates (7–10 week old) weighing approximately 20 g were used (supplied by Charles River) [22]. Animals were housed in cages with environmental enrichment and a 12-h light/dark cycle. Temperature was maintained at approximately 21 °C and mice had access to water and RM1 food pellets (Aston Pharma) *ad libitum*. Animals received a seven-day acclimatisation period prior to

experiments and all animal experiments were performed in accordance with South African (South African National Standard (SANS 10386–2008)) and UK (Animals (Scientific Procedures) Act 1986) guidelines and were approved by the University of Pretoria Animal Ethics Committee and UCB Pharma Animal Welfare and Ethical Review Body. For the pharmacokinetic (PK) study, a single dose of 10 mg/kg mScl hFc or mScl hFc PD, or 4.4 mg/kg mScl were administered intravenously. For the pharmacology study, administered samples comprised recombinant protein and 0.1% rat serum albumin (a blocking agent). The mScl hFc and mScl hFc PD were administered subcutaneously (SC) once a week at 10 mg/kg for 6 weeks. A control group in which 4.4 mg/kg mScl was dosed daily to deliver the molar equivalent of the hFc-containing proteins was included for completeness. PBS control was administered daily to vehicle control groups and on non-treatment days to mScl hFc and mScl hFc PD treated groups. Mice body weights were measured weekly.

2.6. LC-MS/MS detection of recombinant mScl in serum

Surrogate peptides for recombinant mScl proteins were generated using Skyline 20.1 software (MacCoss Lab Software [23]) and the best responding peptides, in terms of liquid chromatography-mass spectrometry (LC-MS/MS) performance, were used to measure serum Scl concentrations. Serum samples were collected at predose, 5 min, 1, 2, 6 h, 1, 2, 3, 4, 5, 6, 7, 8, 10 days for the pharmacokinetic study and at 5, 30 min, 2, 8 h, 1, 7, 42 days for the pharmacology study. Serum, myoglobin internal standard, acetonitrile and 0.2 M tris(2-carboxyethyl)-phosphine were heated at 70 °C for 30 min, followed by addition of 7 µL 0.1 M iodoacetamide and incubation at 37 °C for 30 min in the dark. A 100 mM ammonium bicarbonate buffer (500 µL) and 10 µL resuspended Trypsin (in 50 mM acetic acid) were added to samples, to achieve a 1:78 enzyme to protein ratio, and were incubated in a shaking incubator for minimum of 4 h at 37 °C. Digested samples were desalted using Waters Oasis Hydrophilic-Lipophilic-Balanced solid phase extraction sorbent (Waters Corporation), followed by resuspension in 100 µL 5% MeOH + 0.5% formic acid (FA). Prepared samples were analysed using a Shimadzu UHPLC system coupled to a QTRAP 6500 LC-MS/MS system (AB Sciex). Liquid chromatography was performed using a Phenomenex Luna 3 µ C18 100 Å (150 × 2 mm) HPLC column (Phenomenex). A linear gradient of 2–98% acetonitrile 0.1% FA was applied to elute the peptides at a flow rate of 0.5 mL/min for 5 min. The mass spectrometer was set to run a multiple reaction monitoring experiment for detection of peptides in positive ionization mode. Instrument control and data processing were performed using Analyst 1.6.2 Software (AB Sciex).

2.7. Pharmacokinetic analysis and modelling

LC-MS/MS data from the single dose PK study was fitted to a non-compartmental model and pharmacokinetic parameters were determined using Phoenix WinNonlin 8.1 software (Princeton). For the 42-day prediction model, LC-MS/MS data was fitted to a compartmental model with Berkeley Madonna 9.1.19 software (University of California). Results were used to simulate a 42-day dosage study, assuming 50% bioavailability, 0.1/hour absorption rate and subcutaneous administration [24].

2.8. Bone densitometry and µCT

Whole body areal BMD was determined by dual-energy X-ray absorptiometry (DXA) from isoflurane anaesthetised mice using a Faxitron UltraFocus DXA cabinet (Tucson). All measurements were obtained using the Faxitron Bioptics imaging software. For µCT analysis, the right femur and L5 lumbar vertebrae were cleaned of soft tissue, fixed in 10% neutral buffered formalin for 48 h, then washed and stored in PBS for the duration of the micro computed tomography (µCT) scans. Whole femurs and vertebrae were scanned using the Skyscan 1272 X-ray micro computed tomography instrument (Bruker) and X-ray projection images,

taken with a 0.6° rotation step over 180° sample rotation, were acquired using the Skyscan acquisition software version 1.1.17. X-ray tube was operated at 50 kV source voltage, 200 µA current, 1100 ms exposure time using a 0.5 mm aluminium filter and voxel size of 6 µm (adapted from Ref. [25]). Femurs and vertebrae were reconstructed using Skyscan NRecon version 1.7.4.6 (reconstruction engine: GPUReconServer) with the following settings: Smoothing: 1; Ring artefacts correction: 4; Beam hardening correction: 20% for vertebrae and 30% for femurs. The vertebral body region between the distal and proximal growth plates were selected as region of interest (ROI) for vertebral trabecular analysis. Appearance of the trabecular ‘bridge’ connecting the two primary spongiosa bone ‘islands’ was set as a reference point for analysis of distal femur metaphyseal trabecular bone; an offset of 150 slices (0.9 mm) was applied proximal to the reference point and 500 slices (3 mm) were selected to capture the metaphyseal region for trabecular analysis, with cortical shell excluded. An offset of 430 slices from the reference slice was selected for the femoral cortical bone within the diaphysis with an analysis region of 250 slices (1.5 mm) selected. ROIs were automatically segmented using custom task-list algorithms in CTAn version 1.19.3.1 software (Bruker). Trabecular bone parameters (volumetric bone mineral density (vBMD), bone volume as a percentage of total volume scanned (BV/TV), trabecular thickness (Tb.Th), space (Tb.Sp), number (Tb.N), pattern factor (Tb.Pf), structural model index (SMI) and degree of anisotropy (DA)), were determined using three-dimensional algorithms, whilst cortical bone parameters (BV/TV, tissue (T.Ar), bone (B.Ar) and medullary area (Ma.Ar), tissue (T.Pm), bone (B.Pm), eccentric perimeter (Es.Pm), and cross sectional thickness (Cs.Th)) were calculated using two-dimensional algorithms. Coefficients of variation (CVs) were determined by independently re-analysing the trabecular bone on the same sample six times to account for operator and automated algorithm bias and determine reproducibility of the analysis. Only trabecular bone analysis was chosen, due to the greater margin of error involved in segmenting the ROIs, since the cortical shell shape changes markedly through the region analysed. CVs of each parameter were determined as the ratio between the standard deviation and the mean, and are as follows: BV/TV: 2.53%; Tb.Th: 1.72%; Tb.N: 3.2%, B.Ar: 0.15% and Cs.Th: 0.46%. Representative images were generated using Skyscan NRecon version 1.7.4.6.

2.9. Statistical analysis

Results are presented as mean ± SD. Data comparison was performed with GraphPad Prism 8.4.1 (GraphPad Software) using two-way ANOVA for the bone nodule formation assay, and unpaired t-tests or ordinary one-way ANOVA for trabecular and cortical bone parameters. A p-value of <0.05 was considered significant.

3. Results

3.1. Production of recombinant sclerostin proteins

Recombinant wild type mouse sclerostin (mScl) and two novel recombinant mScl fusion proteins were produced for this study. To increase protein half-life, a DNA construct containing mScl fused with hFc positioned at the mScl C-terminus (mScl hFc) was designed. In a third construct, an eight-aspartate residue motif (PD) was included downstream of the hFc in an attempt to improve the protein's ability to localise to bone (mScl hFc PD). Recombinant proteins were expressed in HEK293 cells and were purified by hFc-tag affinity (for the proteins containing this sequence), cation exchange, and size exclusion chromatography. When analysed by SDS-PAGE under reducing conditions, mScl appeared as a fuzzy band of ~35 kDa (Fig. 1). Monomeric mScl hFc (~50 kDa) was slightly smaller than mScl hFc PD monomers (~55 kDa) (Fig. 1). In non-reducing conditions, the hFc component is expected to form disulphide-linked dimers, and when run on non-reducing SDS-PAGE, bands of a size equivalent to dimeric mScl hFc and mScl hFc PD were observed

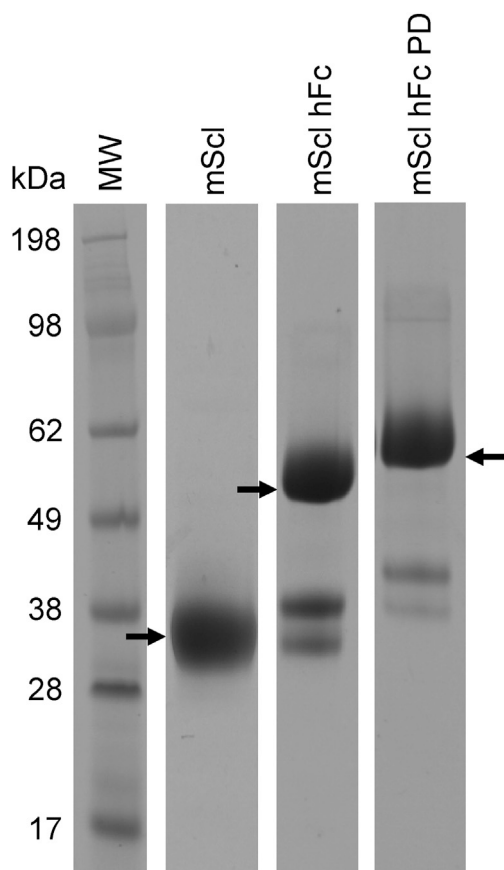


Fig. 1. SDS PAGE of purified mScl, mScl hFc and mScl hFc PD under reduced conditions. Top and lower black arrows pointing to the right: mScl (~35 kDa) and mScl hFc (primary band ~50 kDa). Black arrow pointing to the left: primary band (~55 kDa) for mScl hFc PD. Cropped gels are juxtaposed and complete gels are presented in [Supplementary Fig. S9](#). Lane 4 is from [Supplementary Fig. S9a](#) (lane 8), lane 3 is from [Supplementary Fig. S9b](#) (lane 8), and lanes 1 and 2 are from [Supplementary Fig. S9c](#) (lanes 1 and 6).

([Supplementary Fig. S1](#)). N-terminal sequencing showed that a minor proportion of the mScl hFc PD protein was truncated 176 amino acids downstream from the mScl N-terminus, towards the end of the mScl C-terminal flexible region fused to hFc, resulting in truncation of the majority of the sclerostin sequence from the captured hFc material. Five litre HEK293 culture produced approximately 100 mg purified protein. Endotoxin levels were determined to be < 2 EU/mg, which was considered suitable for *in vitro* and *in vivo* studies.

3.2. Recombinant sclerostin proteins bind to LRP6 and inhibit mineralisation *in vitro*

Since sclerostin normally exists as a monomer, it was important to confirm that the formation of a dimeric molecule did not impair the mScl activity *in vitro*. Sclerostin binds via an Nxl (asparagine-any amino acid-isoleucine) motif to the highly conserved first β -propeller in the extracellular domain of LRP5/6 Wnt co-receptors [20,26]. Therefore, to confirm the functional activity of the recombinant mScl proteins, they were tested *in vitro* for their ability to bind a fragment of LRP6 containing the first and second β -propellers of the receptor extracellular domain [20]. Isothermal titration calorimetry (ITC) demonstrated dose-dependent binding of all three forms of recombinant mScl, with affinities in the nM range: mScl: 147 ± 75 nM (similar to previously reported affinity [27]), mScl hFc: 117 ± 15 nM, and mScl hFc PD: 746 ± 163 nM, indicating moderate to strong interaction with LRP6 ([Fig. 2](#)). Stoichiometries for mScl proteins binding LRP6 were 0.8, 0.6, and 0.9 for mScl, mScl hFc and mScl hFc PD, respectively ([Fig. 2](#)). Dose-dependent binding to LRP6 was confirmed via two orthogonal techniques (surface plasmon resonance competition assay and microscale thermophoresis; [Supplementary Fig. S2 and S3](#)) and together these data confirmed the ability of all three forms of recombinant mScl to bind LRP6.

Sclerostin is a potent negative regulator of bone formation, therefore we tested the ability of the recombinant mScl proteins to inhibit this process using an *in vitro* bone nodule formation assay. MC3T3-E1 cells were selected as an appropriate model since they express LRP4/5/6 and have been shown to be sensitive to sclerostin [28]. Confluent MC3T3-E1 cells treated with osteogenic (OM) media (complete growth medium supplemented with 50 μ g/mL ascorbate-2-phosphate and 10 mM β -glycerophosphate, changed every 2–3 days) differentiated into

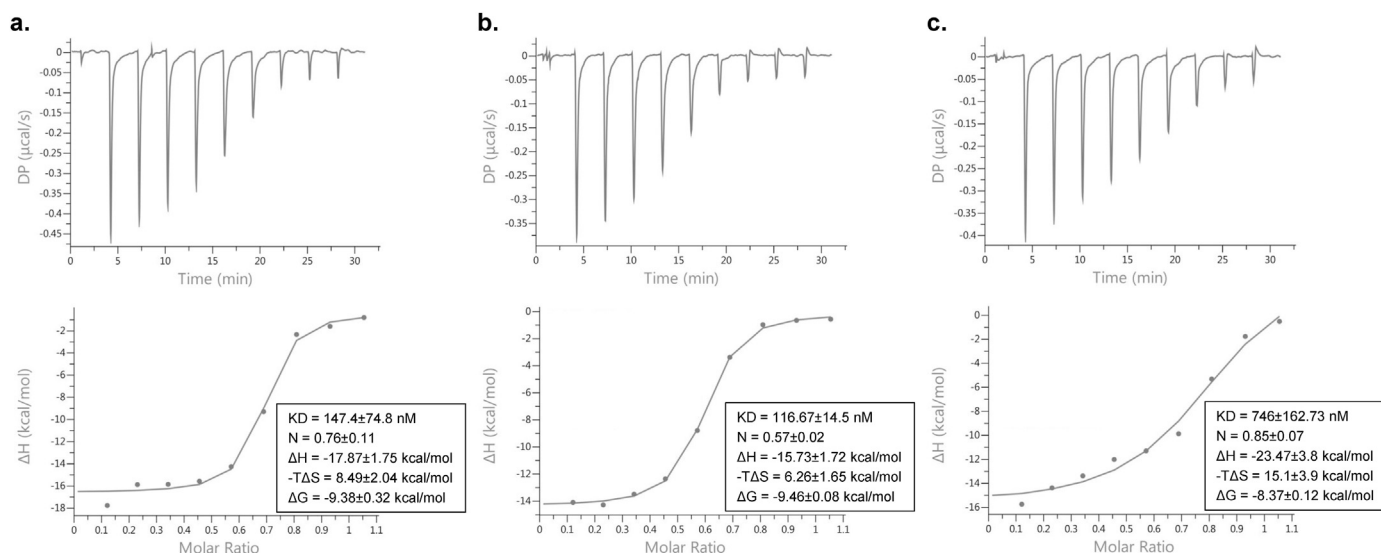


Fig. 2. ITC binding of recombinant mScl constructs to LRP6. (a, b, c) Raw calorimetric data and representative experimental titration curves of mScl (a), mScl hFc (b), and mScl hFc PD (c) binding to LRP6 are shown in the upper and lower panels respectively. Average binding affinities and thermodynamic parameters for three replicates are shown next to the binding isotherms. KD: dissociation constant; N: stoichiometry; ΔH : change in enthalpy; $-\Delta S$: temperature delta entropy; ΔG : change in free energy.

osteoblast-like cells and formed a well-mineralised extracellular matrix that covered $\geq 90\%$ of the plate surface after approximately nine days, consistent with previously reported results [29] (Fig. 3). Mineralisation was visualised by Alizarin Red S staining and quantified following solubilisation with cetylpyridinium chloride (CPC). Substantial inhibition of mineralisation was observed in cells treated with 50 nM of any of the recombinant mScl proteins ($p < 0.0001$) (Fig. 3). Addition of $\sim 5x$ molar excess of sclerostin-neutralising antibody (anti-Scl Ab [21]) confirmed that inhibition was due to functional inhibition by mScl since mineralisation was restored in its presence ($p < 0.0001$), but was unaffected by an irrelevant isotype control antibody (control Ab) ($p < 0.0001$) (Fig. 3). These results, together with data from the three biophysical techniques, suggest that the three recombinant mScl proteins bound competently to the LRP6 Wnt co-receptor, and demonstrated that the proteins

recapitulated the functional effects of wild type sclerostin *in vitro*.

3.3. Pharmacokinetics of recombinant mScl proteins

Next, the pharmacokinetic (PK) properties of the recombinant mScl proteins were assessed in 7–10 week old wild type (WT) and SOST knock out (SOST^{-/-}) mice following a single intravenous (IV) administration of mScl hFc (10 mg/kg), mScl hFc PD (10 mg/kg), or a molar equivalent of mScl (4.4 mg/kg), thereby adjusting for the approximately 4.4-fold difference in protein molecular weights (predicted molecular weights based on amino acid sequence: 94.8 kDa for the hFc fusion proteins vs. 21.5 kDa for mScl). The 10 mg/kg/wk dose was selected based on prior experience of the PK behaviour of Fc-containing proteins. Blood samples were collected at various intervals post-dose to enable quantitation of the

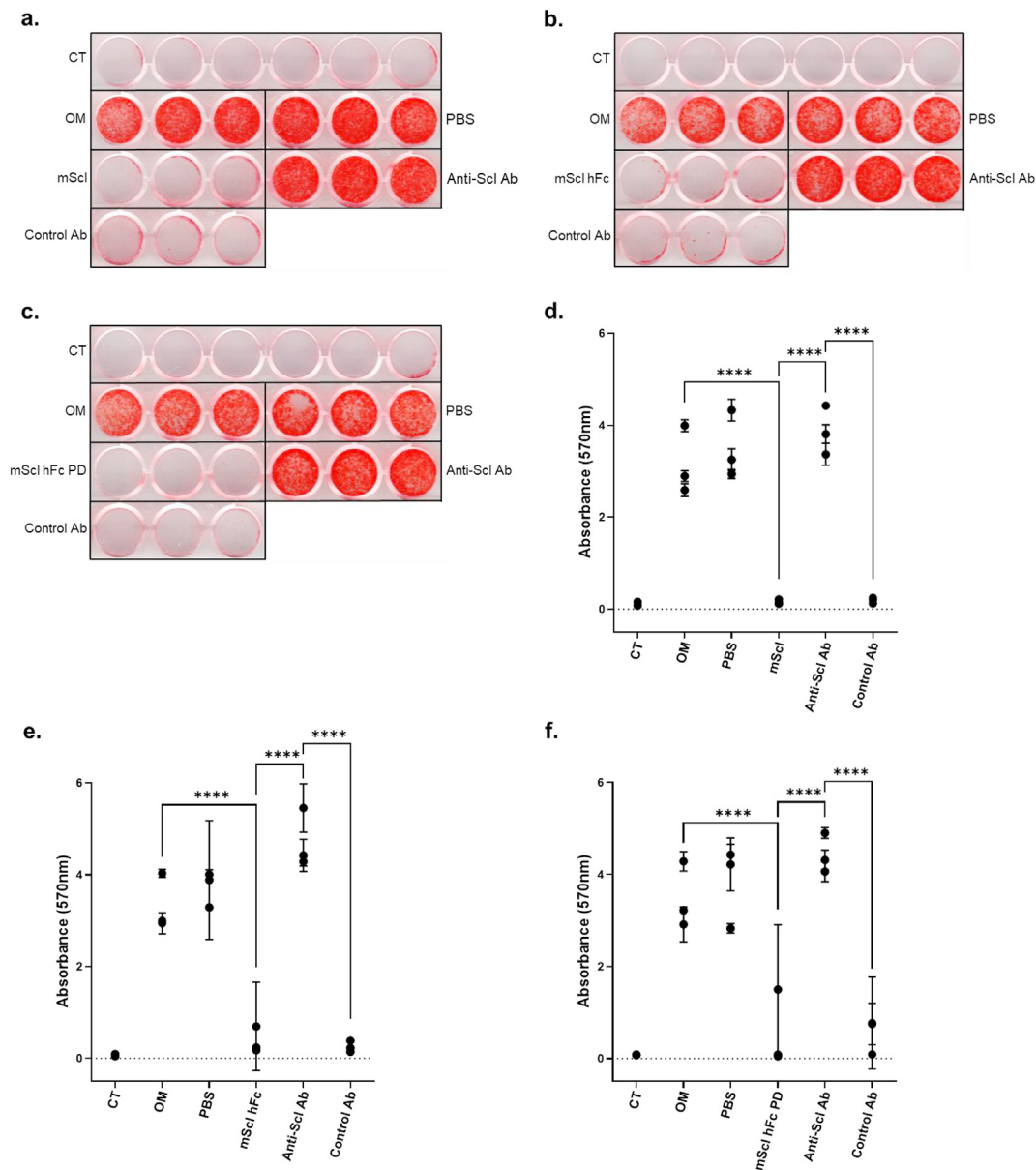


Fig. 3. Recombinant mScl proteins inhibit osteoblast mineralisation. (a, b, c) MC3T3-E1 cells were cultured for nine days and mineral was stained with Alizarin Red S. Cells treated with mScl (a), mScl hFc (b) and mScl hFc PD (c). (d, e, f) Alizarin Red S-stained mineral was solubilised using CPC for quantitative analysis of mineralisation. Absorbance (570 nm) data from three independent experiments was plotted for the three recombinant mScl constructs: mScl (d), mScl hFc (e) and mScl hFc PD (f). CT: complete growth media control; OM: osteogenic media control; PBS: osteogenic media with PBS vehicle control; mScl/mScl hFc/mScl hFc PD: osteogenic media with 50 nM recombinant mScl as indicated; Anti-Scl Ab: osteogenic media with 230 nM anti-Scl Ab and 50 nM of indicated recombinant mScl; Control Ab: osteogenic media with 230 nM irrelevant isotype control Ab and 50 nM of indicated recombinant mScl. All conditions were set up in triplicate, except for CT (6 wells). Mean \pm SD of triplicates from three independent experiments shown. Two-way ANOVA was used for statistical analysis. ****P < 0.0001.

recombinant protein in serum by LC-MS/MS. WT and *SOST*^{-/-} mice gave broadly similar PK profiles for the three recombinant mScl proteins. Native mScl had a very short half-life and was undetectable after 5 min post dose (Supplementary Table 1). As expected, the hFc fusion proteins had an extended half-life, estimated at 1.5–1.8 days for mScl hFc and 4 days for mScl hFc PD (Supplementary Table 1). Compartmental pharmacokinetic analysis of mScl hFc with IV administration fitted two-compartment kinetics. Data from this fitted model was used to simulate a 42-day prediction model for a repeat dose pharmacology study with weekly subcutaneous (SC) dosing of 10 mg/kg hFc fusion proteins: peak and trough simulated mScl hFc concentrations were 2.8–3.2 µg/mL and 0.4–0.5 µg/mL respectively (Supplementary Fig. S4). Since trough levels exceeded previously reported serum sclerostin levels [30,31], these doses were considered suitable for use in the six week repeat dose pharmacology study.

3.4. Effect of recombinant mScl on bone parameters in wild type and *SOST*^{-/-} mice following a 6-week treatment period

Administration of mScl hFc and mScl hFc PD (weekly) or mScl (daily) to young (7–10 week old) female WT and *SOST*^{-/-} mice was well tolerated and body weights were comparable for both genotypes throughout the 6-week study (Supplementary Fig. S5). Whole body areal bone mineral density (aBMD), measured by dual-energy X-ray absorptiometry (DXA), was higher at baseline in *SOST*^{-/-} vs WT mice (80 ± 9 g/cm² vs 100 ± 10 g/cm², *p* < 0.0001), consistent with the previously reported phenotype [22] (Supplementary Fig. S5). For each genotype, whole body aBMD was typically higher at day 40 compared with baseline regardless of the treatment group. Levels of the bone formation marker procollagen type I N-terminal propeptide (P1NP) in terminal bleed samples were comparable between the vehicle and treated *SOST*^{-/-} groups (Supplementary Fig. S6), indicating no significant difference (*p* = 0.196, 0.196 and 0.362 for mScl, mScl hFc and mScl hFc PD, respectively) in bone formation at the time the samples were collected.

The effect of the recombinant mScl proteins on skeletal phenotype of WT and *SOST*^{-/-} mice was analysed by micro-computed tomography (µCT) scanning and 2D and 3D bone histomorphometry following the 42-day treatment period. Consistent with the genotype effect observed by DXA, there was a clear difference in trabecular and cortical parameters of WT compared with vehicle treated *SOST*^{-/-} mice (Table 1; Supplementary Tables 2 and 3).

Administration of mScl hFc PD resulted in a modest but statistically significant effect on trabecular bone parameters of *SOST*^{-/-} mice (Fig. 4; Table 1; Supplementary Table 2). Volumetric BMD (vBMD), bone volume fraction (BV/TV) and trabecular number (Tb.N) in lumbar vertebrae of *SOST*^{-/-} mice treated with mScl hFc PD were approximately 20% (*p* = 0.04), 15% (*p* = 0.04) and 19% (*p* = 0.009) lower compared with the

vehicle control group, whilst trabecular separation (Tb.S) was 27% (*p* = 0.04) higher (Fig. 4, Table 1). In femoral trabecular bone a modest but statistically significant 37% increase in trabecular separation (*p* = 0.02) and non-significant trends towards reduced BV/TV (27%, *p* = 0.10), vBMD (21%, *p* = 0.13), and Tb.N (25%, *p* = 0.08) were observed (Supplementary Fig. S7 and Supplementary Table 2). No significant effects on vertebral and femoral trabecular bone were observed in *SOST*^{-/-} mice treated with mScl or mScl hFc. Femoral cortical indices were comparable across all three proteins tested, and no significant effects were seen in trabecular or cortical bone of any of the WT treated groups. Representative images for lumbar vertebrae and femurs are shown in Fig. 4F and Supplementary Figure S7E.

Pharmacokinetic parameters in the six-week study (measured using serum samples collected at 5, 30 min, 2, 8, 24 h, 7, 42 days) were similar to the single dose pharmacokinetic study. Trough values for the fitted mScl hFc data and the prediction model were also comparable (Supplementary Fig. S4).

4. Discussion

Patients with the rare sclerosing bone dysplasia sclerosteosis experience a variety of clinical manifestations relating to skeletal overgrowth. We hypothesised that sclerostin replacement therapy may reduce bone formation in a mouse model of sclerosteosis. Native mouse sclerostin (mScl) was used as a control and was expected to have a short half-life due to its small size. To increase protein half-life, human Fc (hFc) was fused at the C-terminus of mScl, a method utilised in multiple studies, including FDA and EMA approved drugs [32]. Sclerostin binds the extracellular domains of LRP4/5/6 cell-surface receptors in the skeleton to inhibit bone formation [13]. Fusion of hFc to the C-terminus of mScl was not expected to impair the biological function of mScl, as binding to LRP6 is mediated by a flexible loop region (loop 2) within the central core of the protein and does not involve the highly flexible N- and C-terminal arm regions [20]. Previous studies have shown that addition of a poly-aspartate (PD) motif to a protein promoted efficient delivery to bone, with little influence on other biochemical properties [33,34]. An eight-residue PD motif was therefore attached at the extreme hFc C-terminus of one of the fusion proteins to promote bone localisation.

Functional efficacy of the recombinant proteins was demonstrated through their ability to bind the LRP5/6 Wnt co-receptors with nanomolar affinities, which were consistent with previous reports using human sclerostin [20,27]. The interaction of sclerostin with LRP6 can be used as a surrogate for LRP5-binding since binding occurs through a common mechanism [20]. The biological activity of the recombinant sclerostin proteins was investigated in an *in vitro* bone nodule formation assay with pre-osteoblastic cells (MC3T3-E1). As expected, wild type mScl substantially inhibited mineralisation, consistent with previous

Table 1

Trabecular bone histomorphometry of vertebral body between growth plates of L5 lumbar vertebrae.

	WT								<i>SOST</i> ^{-/-}							
	Vehicle		mScl		mScl hFc		mScl hFc PD		Vehicle		mScl		mScl hFc		mScl hFc PD	
	Mean	SD	Mean	SD	Mean	SD	Mean	SD	Mean	SD	Mean	SD	Mean	SD	Mean	SD
vBMD (g/cm ³)	0.27	0.06	0.32	0.14	0.23	0.11	0.26	0.03	0.64	0.05	0.63	0.07	0.61	0.07	0.51	0.14*
BV/TV (%)	16.21	1.85	17.49	5.66	14.97	3.78	16.14	1.12	29.40	1.83	29.03	2.39	28.47	2.61	24.91	4.92*
Tb.Th (mm)	0.05	0.00	0.05	0.00	0.05	0.00	0.05	0.00	0.06	0.00	0.06	0.00	0.06	0.00	0.06	0.00
Tb.Sp (mm)	0.21	0.02	0.22	0.02	0.25	0.04	0.22	0.01	0.15	0.01	0.15	0.01	0.16	0.03	0.19	0.04*
Tb.N (mm ⁻¹)	3.52	0.20	3.24	0.46	3.10	0.68	3.43	0.19	4.75	0.25	4.61	0.35	4.59	0.39	3.85	0.80**
Tb.Pf (mm ⁻¹)	18.19	3.64	17.26	4.19	17.15	4.01	15.85	1.79	16.53	2.20	15.90	1.73	17.09	4.19	17.34	2.18
SMI	1.37	0.16	1.36	0.22	1.37	0.24	1.26	0.11	1.52	0.12	1.51	0.13	1.55	0.25	1.66	0.21
DA	0.46	0.03	0.49	0.04	0.46	0.03	0.49	0.03	0.24	0.06	0.27	0.05	0.21	0.04	0.27	0.07

Data are expressed as the mean ± SD of *n* = 6 mice/group (except *SOST*^{-/-} vehicle group: *n* = 7). Ordinary one-way ANOVA was performed for statistical analysis: **p* < 0.05; ***p* < 0.01 compared with *SOST*^{-/-} vehicle group. The region of interest was the vertebral body of the L5 lumbar vertebrae. vBMD: volumetric bone mineral density; BV/TV: bone volume fraction; Tb.Th: trabecular thickness; Tb.Sp: trabecular space; Tb.N: trabecular number; Tb.Pf: trabecular pattern factors; SMI: structure model indexes; DA: degree of anisotropy.

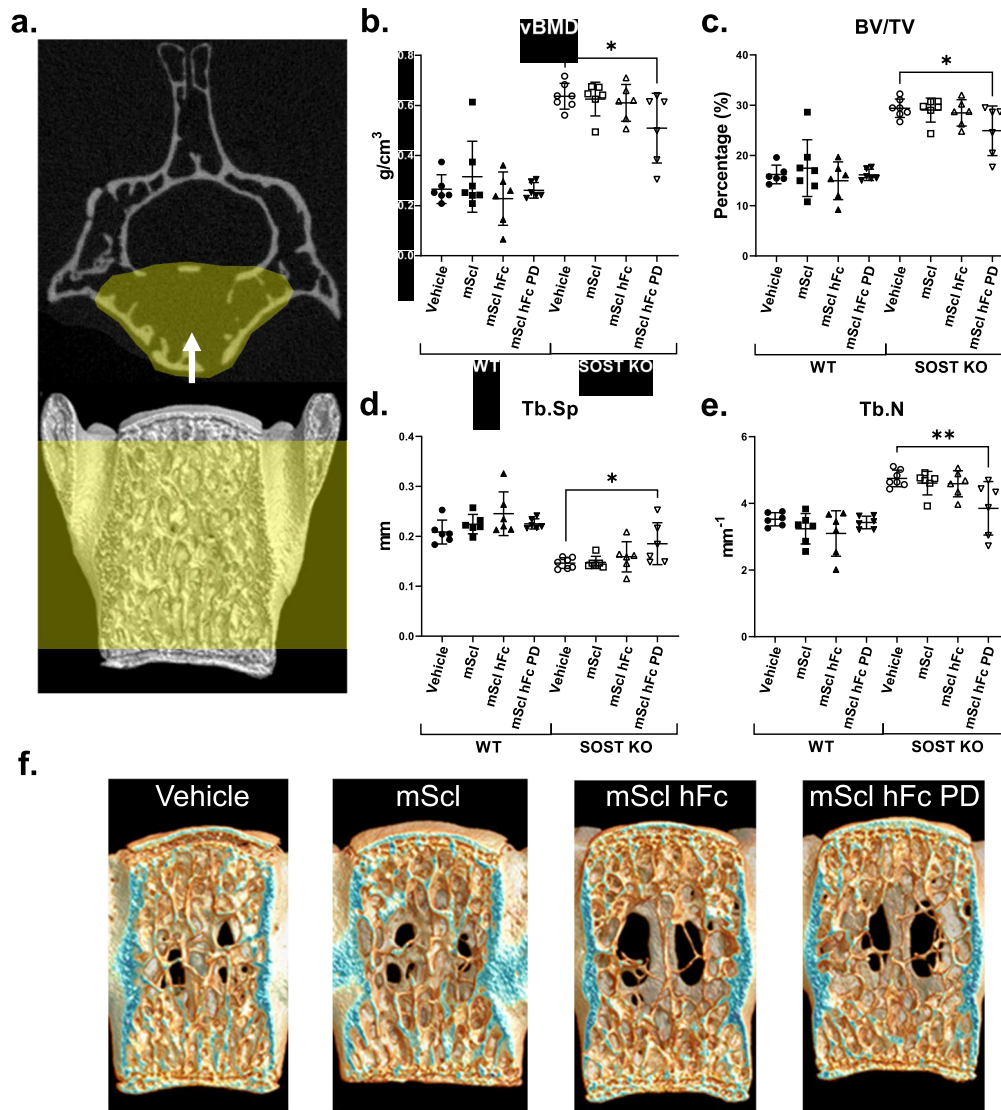


Fig. 4. Vertebral trabecular bone phenotype of WT and $SOST^{-/-}$ mice treated with Vehicle, mScl, mScl hFc and mScl hFc PD. Trabecular microarchitecture was assessed by μ CT in WT and $SOST^{-/-}$ mice aged \sim 3 months. (a) Vertebral body region (top yellow region) between the distal and proximal growth plates (bottom yellow region) was selected as the region of interest for vertebral trabecular analysis. (b, c, d, e) vBMD (b), BV/TV (c), Tb.Sp (d) and Tb.N (e). (f) Representative frontal plane μ CT images of fifth lumbar vertebral body in WT and $SOST^{-/-}$ mice. Vertebral body is viewed from the front (white arrow in (a)). Blue indicates bone density and are for illustration purposes only. Bars represent mean \pm SD of $n = 6$ mice/group (except $SOST^{-/-}$ mice vehicle group: $n = 7$). Ordinary one-way ANOVA was performed for statistical analysis: * $p < 0.05$; ** $p < 0.01$.

reports for rat and human sclerostin [21,28]. This was mirrored by the novel mScl fusions studied here, indicating that mScl with C-terminal hFc retained binding and biological activity, even when dimerised via that hFc. The veracity of this recombinant mScl activity was substantiated by restoration of mineralisation in the presence of a sclerostin neutralising antibody (anti-Scl Ab).

The canonical Wnt signalling pathway has been identified as a critical regulator of bone homeostasis and sclerostin acts as an inhibitor of this pathway [13]. A weakness of the current study is that the impact of the recombinant sclerostin proteins on Wnt pathway activity was not investigated *in vitro*. However, the ability of the sclerostin proteins to bind the LRP6 Wnt co-receptor and their *in vitro* efficacy on MC3T3-E1 mineralisation is consistent with the previously reported behaviour of wild type sclerostin [28] and thus was considered sufficient to warrant testing of the proteins in the $SOST^{-/-}$ mouse model of sclerosteosis.

Although sclerostin has been reported to have effects in non-skeletal tissue, the aim of the current study was to explore the effects of sclerostin

reconstitution on the skeleton as a potential approach to manage excessive bone formation in a model of sclerosteosis. $SOST^{-/-}$ mice phenocopy sclerosteosis and display a high bone mass phenotype that is driven by increased bone formation and rapid increase in BMD as mice grow [22]. In a pharmacokinetic study, a single 10 mg/kg mScl hFc or mScl hFc PD dose, selected based on prior experience of the PK behaviour of Fc-containing proteins, or a single molar equivalent dose of 4.4 mg/kg mScl, adjusting for molecular weight differences between the recombinant proteins, was administered to wild type and $SOST^{-/-}$ mice. Assessment of serum sclerostin levels following administration showed a short (undetectable after 5 min post-dose) and extended half-life for wild type mScl and fusion proteins, respectively. Weekly administration of 10 mg/kg hFc-tagged mScl proteins was simulated in a 42 day model (Supplementary Fig. S4), showing that trough mScl serum levels (0.5–3 μ g/mL) would remain well above previously reported sclerostin serum concentration (<100 pg/mL) and thus could be expected to promote a biological effect [30,31]. For completeness, wild type mScl was

administered to a control group, using daily dosing (to reflect this protein's short half-life), however the rapid clearance of the protein meant that it was unlikely any biological effect would be observed. The effect of sclerostin administration on the skeleton of *SOST*^{-/-} mice was measured by DXA and μ CT. Generalised bone overgrowth is observed in both sclerosteosis patients and *SOST*^{-/-} mice [5,8,22] and assessment of lumbar and femoral trabecular and cortical bone by μ CT are standard procedures in preclinical studies, therefore these bones were examined to understand the extent of any effect following treatment. A small but significant decrease in vBMD, BV/TV, Tb.N, and an increase in Tb.Sp in the vertebral trabecular bone of *SOST*^{-/-} mice treated with mScl hFc PD was observed. In contrast, there was no clear effect on whole body areal BMD or femoral cortical bone following administration of any of the three recombinant mScl proteins. No significant changes in cortical or trabecular bone in response to treatment with any form of sclerostin were observed in control WT mice. A limitation of this study is that no additional techniques were used to evaluate bone properties (e.g. histomorphometry or biomechanical testing). However, high-resolution μ CT analysis has the advantage of evaluating the 3D structural microarchitecture in a larger section of bone, rather than being subjective to a single slice analysis with histology, and should therefore be sufficient for analysing the effect of the recombinant sclerostin on bone microarchitecture.

There are several possibilities for the limited efficacy observed in this study. We first considered whether the study may have been limited by a too short treatment period, however, the six-week study should have allowed 2–3 bone remodelling cycles, which should have been sufficient to see changes in trabecular parameters [35]. Secondly, sclerosteosis usually stabilises when patients reach skeletal maturity in the third decade of life [2], thus, treatment may be most effective when started in young individuals. It is possible that a greater response might have been seen if treatment was started in younger mice, therefore mouse age might have been a shortcoming in this study. Thirdly, protein immunogenicity could reduce efficacy through production of anti-drug antibodies (ADAs), however ADAs were only rarely observed in treated animals (Supplementary Fig. S8) and there was no difference in bone parameters in mice with, versus mice without, ADAs. Finally, and most importantly, the levels of recombinant mScl may have been too low to achieve sufficient efficacy, or the protein may not have reached the bone tissue, where sclerostin is normally produced and acts [10]. Serum mScl levels were in excess of previously reported circulating concentrations in mice [30,31]. Although protein affinity of recombinant mScl was in the nanomolar range, occupancy of LRP5/6 may have been insufficient to elicit robust inhibition of Wnt signalling in bone tissue. Furthermore, it is possible that systemic administration did not deliver the recombinant proteins to the target tissue efficiently. Since small effects were seen in the group administered with mScl hFc PD, inclusion of the bone targeting moiety may have been beneficial, although the current study did not explore whether the protein localised to bone tissue.

A bigger response may be achieved by significantly increasing the dose (e.g. 10x), however protein solubility and maximum injection volume may limit the feasibility of this approach. A bone-targeting, mScl-expressing adeno-associated virus would be an interesting proof of concept for a means to express the mScl proteins within the skeleton thus circumventing limitations of recombinant protein production and administration [36].

Administration of recombinant mScl hFc PD protein partially corrected the high bone mass phenotype of the *SOST*^{-/-} mouse, suggesting that bone-targeting of sclerostin engineered to improve half-life was able to negatively regulate bone formation in the *SOST*^{-/-} mouse model of sclerosteosis. However, the modest efficacy indicates that sclerostin replacement may not be an optimal strategy to mitigate excessive bone formation in sclerosteosis. Alternative approaches such as new and improved sclerostin constructs, sclerostin gene therapy, or other strategies to inhibit Wnt signalling in bone could be explored. Further research is certainly warranted as a treatment for this debilitating, sometimes fatal

condition that currently relies on difficult and protracted surgical measures for disease management and would dramatically improve the quality of life of these patients and their families.

Funding and support

This work was supported by UCB Pharma (Slough, UK), private funders, University of Pretoria (Pretoria, RSA), and the National Research Foundation (NRF). Opinions expressed and conclusions arrived at, are those of the author and are not necessarily to be attributed to the NRF.

Declaration of competing interest

MS, CD, KG, MP, PC, AK, HZK and GH are/have been employees of UCB Pharma and may hold UCB Pharma shares and/or stock options. TD and VN declare no competing interests.

Acknowledgements

The authors gratefully acknowledge the contributions of Drs Chiara Valenzano, Sherri Dudal, Jeff Kennedy, Alison Turner, Mr Joby Jose, and Mr Phil Stanley for sharing their technical expertise, and to Dr Alistair Henry and many others in UCB Early Solutions for their insights and expertise. Thank you also to Mr Phil Salmon (Bruker MicroCT) for assisting with the configuration and development of the automated analysis module for μ CT analysis. Further gratitude is extended to Prof. Jacques Theron and Ms Andale Conradie (Department of Microbiology and Plant Pathology), and Prof. Lyndy McGaw (co-supervisor) and Ms Annette Venter (Department of Paraclinical Sciences) at University of Pretoria, for their lab assistance, insight, and support. A special thank you to Prof. Socrates Papapoulos for pushing for this project to go ahead and tremendous support throughout.

Author contributions

TD, HZK, GH and VN conceptualised the study and formulated the overarching research goals and aims. TD, MS, CD, KG, AK, MP, PC and GH were responsible for development and design of methodology. Experiments and data collection were performed by TD, MS, CD, KG, AK, and PC, whilst statistical analysis was done by TD and MP. TD validated experiments/results and curated the data. The original draft was prepared by TD and revisions and final editing were done by GH and TD. The study was supervised by VN and GH, who was also the project administrator. All authors read and approved the final manuscript.

Appendix A. Supplementary data

Supplementary data to this article can be found online at <https://doi.org/10.1016/j.jot.2021.05.005>.

References

- [1] Beighton P, Hamersma H. Sclerosteosis in South Africa. *South Afr Med J Suid-Afr Tydskrif Vir Geneeskde* 1979;55:783–8.
- [2] van Lierop AH, Appelman-Dijkstra NM, Papapoulos SE. Sclerostin deficiency in humans. *Bone* 2017;96:51–62. <https://doi.org/10.1016/j.bone.2016.10.010>.
- [3] Beighton P, Durr L, Hamersma H. The clinical features of Sclerosteosis: A Review of the manifestations in twenty-five affected individuals. *Ann Intern Med* 1976;84:393–7. <https://doi.org/10.7326/0003-4819-84-4-393>.
- [4] du Plessis JJ. Sclerosteosis: neurosurgical experience with 14 cases. *J Neurosurg* 1993;78:388–92. <https://doi.org/10.3171/jns.1993.78.3.0388>.
- [5] Gardner JC, van Bezooijen RL, Mervis B, Hamdy NAT, Löwik CWGM, Hamersma H, et al. Bone mineral density in sclerosteosis; affected individuals and gene carriers. *J Clin Endocrinol Metab* 2005;90:6392–5. <https://doi.org/10.1210/jc.2005-1235>.
- [6] Hamersma H, Gardner J, Beighton P. The natural history of sclerosteosis. *Clin Genet* 2003;63:192–7.
- [7] Hamersma H, Hofmeyr L. Too much bone: the middle ear in sclerosing bone dysplasias. *Adv Oto-Rhino-Laryngol* 2007;65:61–7. <https://doi.org/10.1159/000098673>.

- [8] van Lierop AH, Hamdy NA, Hamersma H, van Bezooijen RL, Power J, Loveridge N, et al. Patients with sclerosteosis and disease carriers: human models of the effect of sclerostin on bone turnover. *J Bone Miner Res* 2011;26:2804–11. <https://doi.org/10.1002/jbmr.474>.
- [9] Balemans W, Van Den Ende J, Freire Paes-Alves A, Dikkers FG, Willems PJ, Vanhoenacker F, et al. Localization of the gene for sclerosteosis to the van Buchem disease–gene region on chromosome 17q12–q21. *Am J Hum Genet* 1999;64:1661–9. <https://doi.org/10.1086/302416>.
- [10] Ke HZ, Roberts SJ, Holdsworth G. Chapter 74 - pharmacologic basis of sclerostin inhibition. In: Bilezikian JP, Martin TJ, Clemens TL, Rosen CJ, editors. *Princ. Bone Biol.* 4th ed. Academic Press; 2020. p. 1711–31. <https://doi.org/10.1016/B978-0-12-814841-9.00074-9>.
- [11] Brunkow ME, Gardner JC, Van Ness J, Paepfer BW, Kovacevich BR, Proll S, et al. Bone dysplasia sclerosteosis results from loss of the SOST gene product, a novel cystine knot-containing protein. *Am J Hum Genet* 2001;68:577–89.
- [12] Balemans W, Ebeling M, Patel N, Van Hul E, Olson P, Dioszegi M, et al. Increased bone density in sclerosteosis is due to the deficiency of a novel secreted protein (SOST). *Hum Mol Genet* 2001;10:537–44. <https://doi.org/10.1093/hmg/10.5.537>.
- [13] Holdsworth G, Roberts SJ, Ke HZ. Novel actions of sclerostin on bone. *J Mol Endocrinol* 2019;62:R167–85. <https://doi.org/10.1530/JME-18-0176>.
- [14] Nusse R, Clevers H. Wnt/ β -Catenin signaling, disease, and emerging therapeutic modalities. *Cell* 2017;169:985–99. <https://doi.org/10.1016/j.cell.2017.05.016>.
- [15] Lin C, Jiang X, Dai Z, Guo X, Weng T, Wang J, et al. Sclerostin mediates bone response to mechanical unloading through antagonizing wnt/ β -catenin signaling. *J Bone Miner Res* 2009;24:1651–61. <https://doi.org/10.1359/jbmr.090411>.
- [16] Aledort L, Ljung R, Mann K, Pipe S. Factor VIII therapy for hemophilia A: current and future issues. *Expet Rev Hematol* 2014;7:373–85. <https://doi.org/10.1586/17474086.2014.899896>.
- [17] Peters R, Harris T. Advances and innovations in haemophilia treatment. *Nat Rev Drug Discov* 2018;17:493–508. <https://doi.org/10.1038/nrd.2018.70>.
- [18] Eschbach JW, Egrie JC, Downing MR, Browne JK, Adamson JW. Correction of the anemia of end-stage renal disease with recombinant human erythropoietin. Results of a combined phase I and II clinical trial. *N Engl J Med* 1987;316:73–8. <https://doi.org/10.1056/NEJM198701083160203>.
- [19] Ke HZ, Richards WG, Li X, Ominsky MS. Sclerostin and dickkopf-1 as therapeutic targets in bone diseases. *Endocr Rev* 2012;33:747–83. <https://doi.org/10.1210/er.2011-1060>.
- [20] Holdsworth G, Slocombe P, Doyle C, Sweeney B, Veverka V, Le Riche K, et al. Characterization of the interaction of sclerostin with the low density lipoprotein receptor-related protein (LRP) family of Wnt Co-receptors. *J Biol Chem* 2012;287:26464–77. <https://doi.org/10.1074/jbc.M112.350108>.
- [21] Veverka V, Henry AJ, Slocombe PM, Ventom A, Mulloy B, Muskett FW, et al. Characterization of the structural features and interactions of sclerostin. *J Biol Chem* 2009;284:10890–900. <https://doi.org/10.1074/jbc.M807994200>.
- [22] Li X, Ominsky MS, Niu Q-T, Sun N, Daugherty B, D'Agostin D, et al. Targeted deletion of the sclerostin gene in mice results in increased bone formation and bone strength. *J Bone Miner Res* 2008;23:860–9. <https://doi.org/10.1359/jbmr.080216>.
- [23] MacLean B, Tomazela DM, Shulman N, Chambers M, Finney GL, Frewen B, et al. Skyline: an open source document editor for creating and analyzing targeted proteomics experiments. *Bioinformatics* 2010;26:966–8. <https://doi.org/10.1093/bioinformatics/btq054>.
- [24] Krause A, Lowe PJ. Visualization and communication of pharmacometric models with Berkeley Madonna. *CPT Pharmacometrics Syst Pharmacol* 2014;3:e116. <https://doi.org/10.1038/psp.2014.13>.
- [25] Shah M, Kola B, Bataveljic A, Arnett TR, Viollet B, Saxon L, et al. AMP-activated protein kinase (AMPK) activation regulates in vitro bone formation and bone mass. *Bone* 2010;47:309–19. <https://doi.org/10.1016/j.bone.2010.04.596>.
- [26] He X, Semenov M, Tamai K, Zeng X. LDL receptor-related proteins 5 and 6 in Wnt/ β -catenin signaling: arrows point the way. *Development* 2004;131:1663–77. <https://doi.org/10.1242/dev.01117>.
- [27] Kim J, Han W, Park T, Kim EJ, Bang I, Lee HS, et al. Sclerostin inhibits Wnt signaling through tandem interaction with two LRP6 ectodomains. *Nat Commun* 2020;11:5357. <https://doi.org/10.1038/s41467-020-19155-4>.
- [28] Li X, Ominsky MS, Warmington KS, Morony S, Gong J, Cao J, et al. Sclerostin antibody treatment increases bone formation, bone mass, and bone strength in a rat model of postmenopausal osteoporosis. *J Bone Miner Res Off J Am Soc Bone Miner Res* 2009;24:578–88. <https://doi.org/10.1359/jbmr.081206>.
- [29] Wang D, Christensen K, Chawla K, Xiao G, Krebsbach PH, Franceschi RT. Isolation and characterization of MC3T3-E1 preosteoblast subclones with distinct in vitro and in vivo differentiation/mineralization potential. *J Bone Miner Res* 1999;14:893–903. <https://doi.org/10.1359/jbmr.1999.14.6.893>.
- [30] Shahnazari M, Dwyer D, Chu V, Asuncion F, Stolina M, Ominsky M, et al. Bone turnover markers in peripheral blood and marrow plasma reflect trabecular bone loss but not endocortical expansion in aging mice. *Bone* 2012;50:628–37. <https://doi.org/10.1016/j.bone.2011.11.010>.
- [31] Jastrzebski S, Kalinowski J, Stolina M, Mirza F, Torreggiani E, Kalajcic I, et al. Changes in bone sclerostin levels in mice after ovariectomy vary independently of changes in serum sclerostin levels. *J Bone Miner Res Off J Am Soc Bone Miner Res* 2013;28:618–26. <https://doi.org/10.1002/jbmr.1773>.
- [32] Kontermann RE. Half-life extended biotherapeutics. *Expet Opin Biol Ther* 2016;16:903–15. <https://doi.org/10.1517/14712598.2016.1165661>.
- [33] Nishioka T, Tomatsu S, Gutierrez MA, Miyamoto K, Trandafirescu GG, Lopez PLC, et al. Enhancement of drug delivery to bone: characterization of human tissue-nonspecific alkaline phosphatase tagged with an acidic oligopeptide. *Mol Genet Metabol* 2006;88:244–55. <https://doi.org/10.1016/j.ymgme.2006.02.012>.
- [34] Whyte MP, Greenberg CR, Salman NJ, Bober MB, McAlister WH, Wenkert D, et al. Enzyme-replacement therapy in life-threatening hypophosphatasia. *N Engl J Med* 2012;366:904–13. <https://doi.org/10.1056/NEJMoa1106173>.
- [35] Weinstein RS, Jilka RL, Parfitt AM, Manolagas SC. Inhibition of osteoblastogenesis and promotion of apoptosis of osteoblasts and osteocytes by glucocorticoids. Potential mechanisms of their deleterious effects on bone. *J Clin Invest* 1998;102:274–82. <https://doi.org/10.1172/JCI2799>.
- [36] Yang Y-S, Xie J, Wang D, Kim J-M, Tai PWL, Gravalles E, et al. Bone-targeting AAV-mediated silencing of *Schnurri-3* prevents bone loss in osteoporosis. *Nat Commun* 2019;10:2958. <https://doi.org/10.1038/s41467-019-10809-6>.